Partial Discharge Investigation under Low Air Pressure and Variable Frequency for More-electric-aircraft

Jun Jiang, Bendong Zhang, Zhi Li, and **Chaohai Zhang**
Nanjing University of Aeronautics and Astronautics
Center for more-electric-aircraft power system
Nanjing, China

Prem Ranjan
The University of Manchester
Department of Electrical & Electronic Engineering
Manchester, UK

Xiang Zhang
Manchester Metropolitan University, Manchester
Department of Engineering
Manchester, UK

ABSTRACT

More-electric-aircrafts (MEAs) are heading towards larger power, higher voltage, and more optimum architectures, it is extremely important to understand partial discharge (PD) behaviors under the challenging aeronautical power systems. PD under the pressure of 1–101 kPa and frequency of 50–1000 Hz is studied to emulate the practical situation with the consideration of insulation defects from electric machine windings. The high frequency current transformer (HFCT) is specifically employed to pick up partial discharge signals. Experimental results indicate that PD inception voltage (PDIV) decreases almost linearly with air pressure. As to the discharge amplitude, it increases first and then decreases as air pressure dropping. The highest discharge repetition rate and the number of discharges appear at 30 kPa. High frequency doubles the number of discharges without affecting PD amplitude. Low air pressure causes the phase shift and phase width of the phase-resolved partial discharge (PRPD) to increase, and the trend also is accelerated by high frequency. This experimental approach is beneficial to provide prerequisite knowledge in characterizing PD and assessing its potential adverse impact on the aeronautical power system and consequently contribute to optimizing the insulation design for MEA.

Index Terms — **more-electric-aircraft (MEA), partial discharge (PD), high voltage, aeronautical power system, insulation**

1 INTRODUCTION

THE aviation industry releases more than 900 million metric tons of CO_2, which already accounts for about 2% of total global CO_2 emission and about 12% of the CO_2 emission of all transportation sources [1]. In order to reduce the emissions caused by fuel burning, a considerable improvement in system efficiency is necessary [2–4]. One feasible solution is to increase the use of electric energy, and more-electric-aircraft (MEA) has emerged to power more equipment with increasing electrical capacity. Usually, there are two main schemes to improve electrical capacity: increase the current or the voltage. Raising the current requires thicker conductor diameter leading to an increased flight weight, which is uneconomical. Therefore, increasing the voltage is practical. As an example, the voltage in Boeing B787 has been raised to 540 V, more than twice of that of the previous one [5, 6]. In the future, the operating voltage of aircraft is prone to reach up to several kV to achieve higher power and energy density [7–9]. However, high voltage exposes insulation risks, causing partial discharge (PD), even insulation breakdown. Therefore, it is necessary to evaluate insulation issue in advance for high voltage, high power conditions to ensure the reliable operation of MEA, which was not a possibility in conventional aircrafts.

In order to avoid the breakdown of MEA insulation system, the insulation aging and lifetime under different environmental

parameters have been concerned. Sili *et al* explored the influence of temperature, air pressure and humidity on the typical insulation medium, polyimide, pointing out that the discharge energy exerted an impact on the dielectric strength [10]. The validity of lifetime models of polymers under electrical discharge in aeronautical environment has also been confirmed [11]. However, it is not enough to explore the material life under different parameters, which does not provide sufficient early warning and evaluation information for MEA insulation system. Therefore, the calculation and measurement of PD inception voltage (PDIV) for a variety of aviation cables were explored [12, 13], and a method based on the minimum PDIV is proposed to quantify the insulation performance of the cables. PDIV between turn-to-turn discharge in electrical machines is also paid attention, and PDIV model considering air pressure and temperature is built [14, 15]. Although PDIV is an important electric feature for design of cables and electrical machines, insulation evaluation based on PDIV alone leads to inaccurate results, and more PD statistical features still need to be addressed for evaluation. So, the discharge amplitude and number at low pressure were observed in [16] based on three twisted pairs of winding wire, and both PD magnitude and number of discharges increase as the air pressure decreases. It was also found that the low pressure resulted in peaks shifting to lower phase of 3D φ-n-q [17]. Further, the classification and separation of different PD sources in electric machine were realized based on the discharge characteristics at low pressure, including surface charge, number, and phase [18]. However, the above research is carried out at low frequency, 50/60 Hz, which is not consistent with the variable operation frequency in MEA and more statistical features are still needed to be investigated for insulation evaluation.

In terms of the frequency-induced insulation in MEA, the PD performance of four test objects was examined under high voltage at varying frequencies of both sine and square waveforms [19]. The insulation damage attributed to partial discharges significantly increased as frequency rose. An optical technique was proposed to investigate frequency-related PD activities ranging from 50–1000 Hz given MEA application [20]. However, both tests were conducted at sea level, and the PD behaviors at low pressure due to high flight altitude are not concerned. Therefore, different combinations of low pressure and variable frequencies need to be addressed for practical aeronautical power system in more-electric-aircrafts.

In order to investigate the discharge activities for the special working conditions of present and future MEA, a specialized experiment platform of typical insulation defect is established, and the measurement procedures are illustrated in Section 2. In Section 3, the PDIV, discharge amplitude, discharge number and phase-resolved partial discharge (PRPD) are analyzed to investigate the combined influence of air pressure and frequency. Furthermore, the discharge mechanism and explanation of low air pressure are explored in Section 4. Finally, in Section 5, the main conclusions are drawn. It is expected to provide reference for the PD analysis and insulation design in future MEA towards high power and high voltage.

2 EXPERIMENTAL LAYOUT AND STEPS

2.1 EXPERIMENTAL PLATFORM

The partial discharge detection system is mainly composed of four parts: high voltage power supply, discharge chamber, data acquisition, and air pressure control units, as shown in Figure 1. The high voltage source was used to generate the voltage required by the testing, consisting of a function generator and a high voltage power amplifier. The discharge chamber was used to simulate the insulation defects at required constant air pressure with regard to different flight altitudes. The data collection is used for recording discharge pulses, air pressure, temperature, and humidity values. The partial discharge pulses are detected by a high frequency current transformer (HFCT), its detection bandwidth is 0.3–100 MHz. The output voltage is greater than 10 mV while the current through the HFCT is 1 mA. Finally, the air pressure control module is made up of a vacuum pump and a needle valve.

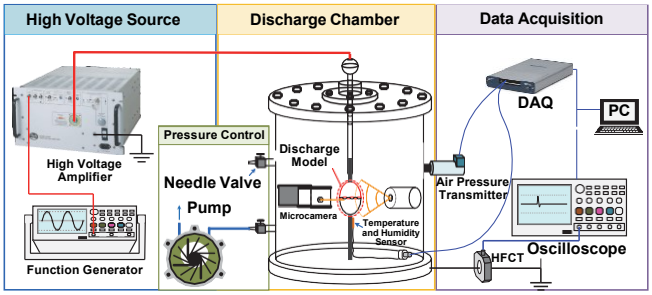

Figure 1. Partial discharge test system of wiring insulation for MEA.

2.2 FAILURE AND SIMULATION

Many power supply machines controlled by pulse width modulation (PWM) are used in the MEA to complete various operations. It is well known that the turn-to-turn insulation in electric machines is easy to break down due to faster switching of PWM, which has become a typical insulation challenge in MEA. In order to simulate a typical insulation failure in MEA, a twisted-pair magnet wires model was made to explore the influence of air pressure and frequency. The fault model refers to IEC 60851-5 standard, and the winding process is illustrated in Figure 2.

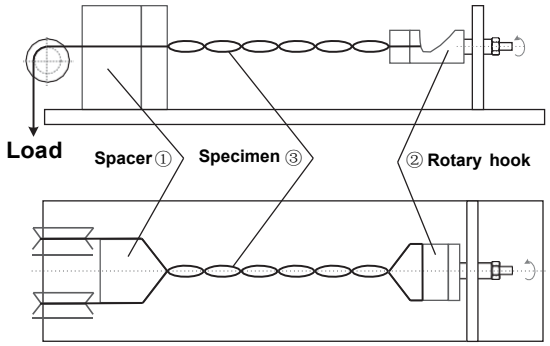

Figure 2. Winding process of twisted pair fault model.

Polyimide was selected as the insulating material for its excellent insulation and temperature resistance, which is widely

used in the power system in aircrafts. Copper enameled wire (dia. 0.51 mm) insulated with polyimide of 0.025 mm thickness was used, with a temperature tolerance up to 180 ℃. Prior to winding the model, the wire was wiped and dried with alcohol paper to eliminate the influence of static electricity and impurities on the surface. According to IEC 60851-5, the two magnet wires were twisted 6 times for a distance of 60 mm with the load of 7 N.

2.3 FREQUENCY AND AIR PRESSURE PARAMETER SELECTION

Since introduced in the 1960s, the voltage levels of 115 V AC at 400 Hz and 28 V DC were commonly used in commercial aircrafts. Until 2009, the Boeing 787 cancelled the constant speed device of the generator, and the frequency of voltage goes up to 360–800 Hz. In the future, the voltage and frequency of MEA is expected to increase up to kilo-volt and kilo-herz, respectively. Therefore, 50 Hz, 400 Hz, 800 Hz and 1 kHz are selected during the testing, wherein, 50 Hz is used for the reference at power frequency.

The air pressure is determined by flying altitude of MEA. The altitude of most commercial aircrafts is about 10 km. Some special-purpose aircrafts, such as F-35, have a maximum altitude of about 25 km. So, Equation (1) is used to detail the air pressure at different heights [21]:

$$h = \frac{T_0}{\tau}\left[\left(\frac{p(0)}{p(h)}\right)^{R\tau} - 1\right] \quad (1)$$

where h is altitude; $p(h)$ is the air pressure at altitude h; $p(0)$ is ground air pressure, which is 101.3 kPa; T_0 is normal temperature, which is 288.15 K; τ and R are constant coefficients with values of 6.5 × 10^{-3} K/m and 29.27 m/K, respectively.

According to Equation (1), the pressure at different heights is shown in Figure 3. As the altitude rises, the air pressure gradually decreases. The air pressure is below 10 kPa at the altitude of 25 km. In order to keep an appropriate margin, the lowest air pressure was chosen as 1 kPa. Therefore, the following air pressure points are selected in the experiment: 101 kPa (1 bar), 80 kPa (0.8 bar), 50 kPa (0.5 bar), 30 kPa (0.3 bar), 10 kPa (0.1 bar) and 1 kPa (0.01 bar).

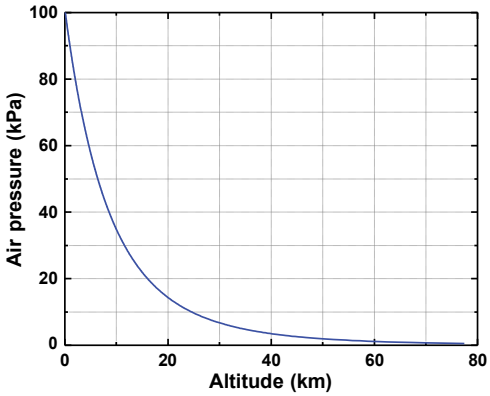

Figure 3. Air pressure at different altitudes.

2.4 MEASUREMENT PROCEDURE

Measurement procedures mainly include PDIV measurement and discharge pulses acquisition. The PDIV automatic measurement system was designed to reduce errors as much as possible. The program control schematic diagram is shown in Figure 4. The function generator is controlled by a Personal Computer (PC) to realize automatic adjustment of the output voltage. HFCT and oscilloscope signals are sent to the PC for detecting discharge pulses. At the beginning, the applied voltage is increased to 70% of the excepted PDIV and slowly raise in a step of 100 V. Each voltage step is maintained for 30 s. If there are PD pulses within 30 s, the voltage is record, if not, continue to increase the voltage until the discharge occurs. The measurement procedure was repeated 5 times, and the average value of voltage recorded was taken as the final PDIV value.

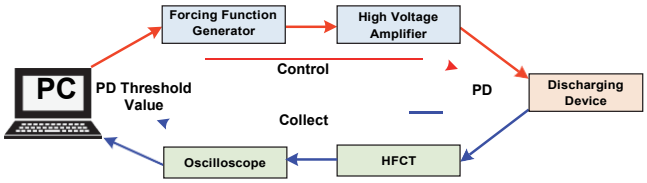

Figure 4. PDIV automatic measurement program.

The discharge pulses acquisition was carried out according to Figure 5. The peak-to-peak value of applied voltage was set to 2.5 kV unchanged while frequency of voltage and air pressure are varied considering the voltage grade of MEA in future and the stability of discharge. In order to avoid the influence of temperature and humidity on the experimental results, the temperature was limited to room temperature and the relative humidity was also limited to a constant. First, frequency was adjusted to 50 Hz, which aims to collect discharge pulses under different air pressure. Then voltage frequency was changed, and the above steps were repeated until all frequencies and air pressures were measured. PD data for 200 consecutive cycles under each condition was saved. Finally, all data was stored in the PC for further PD analysis. In order to avoid the aging effect of the sample under long-time discharge, different winding samples were used at each frequency, and a total of four winding samples were used for PD test. Each winding sample is made in strict accordance with the standard rules to ensure sample consistency.

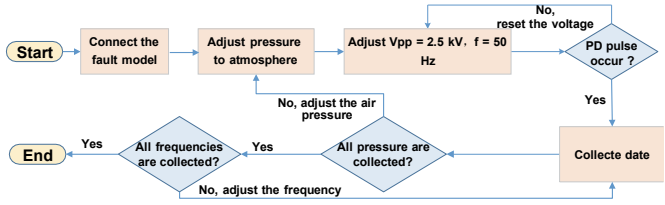

Figure 5. Experimental data collection flowchart.

3 EXPERIMENTAL RESULTS

3.1 PDIV AT DIFFERENT PRESSURES AND FREQUENCIES

The PDIV under different air pressure and frequency is shown in Figure 6. PDIV has an upward trend with increasing

air pressure at various frequencies. PDIV at 1 kPa is less than 50% of PDIV at atmospheric pressure. This emphasizes that PD pulses are more prone to occur at low air pressure. The PDIV at various frequencies is relatively similar, except that the PDIV at 400 Hz is slightly higher than other frequencies. This means PDIV between windings of electric machine is insensitive to the voltage frequency. The significant findings from these tests are the clear reduction in the level of PDIV caused by low air pressure and the weak impact of supply frequency. When PDIV of MEA insulation system is measured, more attention should be paid to air pressure rather than frequency.

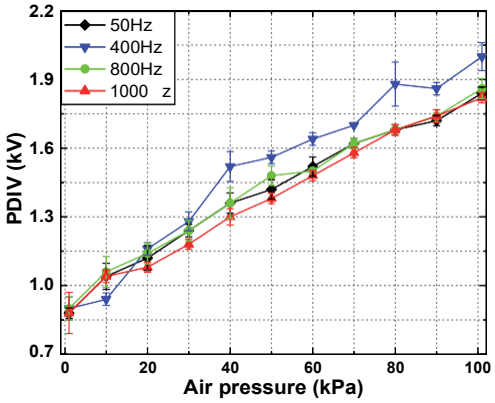

Figure 6. PDIV versus air pressure under different frequencies.

The reason for the influence of air pressure on PDIV is easy to know that the mean free path of electrons λ is the main factors affecting PDIV. According to the ideal gas law, the amount of charge in the air decreases at low pressure, which decreases the probability of electron collision, and increases λ, which is proportional to T/p [22], as shown in Equation (2). With increasing the mean free path λ, the average electron energy increase is higher. So, electron impact at low air pressure has higher energy, which is more likely to cause collision ionization:

$$\lambda=\lambda_0 \frac{p_0}{p}\frac{T}{T_0} \quad (2)$$

where p_0 is atmospheric pressure, 101.3 kPa and T_0 is room temperature, 298.15 K.

3.2 AMPLITUDE AND NUMBER OF PD AT DIFFERENT AIR PRESSURE AND FREQUENCIES

The PD data was subjected to noise reduction processing and discharge pulses are extracted based on MATLAB, as shown in Figures 7–9. Average discharge amplitude versus air pressure at different frequencies is shown in Figure 7. It reveals that with the decrease of air pressure, there is a trend of first increasing and then dropping in discharge amplitude at 50 Hz. The PD amplitude is much smaller at 1 kPa. The average discharge amplitude at the frequency of 400 Hz–1 kHz decrease with the decrease of air pressure, and the reduction rate is much faster at 1–10 kPa. It is interesting to see that the average discharge amplitude at 50 Hz is higher than the other frequencies in the figure, and the difference at 400–1000 Hz is relatively small.

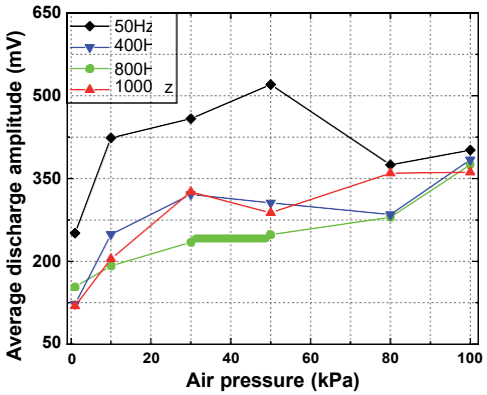

Figure 7. Average discharge amplitude versus air pressure under different frequencies.

The cumulative discharge amplitude PD is closely related to the life of the insulation. Therefore, the total discharge amplitude per second under different frequencies and pressures was calculated, as shown in Figure 8. As the air pressure decreases, the total discharge amplitude shows an inconsistent trend. In the pressure range of 30–101 kPa, the total discharge amplitude gradually increases as the pressure decreases with highest peak at 30 kPa. It means that the insulation damage caused by PD at 30 kPa is much serious than atmospheric pressure in MEA. The discharge trends at different frequencies are inconsistent under the pressure of 1–10 kPa. With the decrease of air pressure at 50 Hz and 400 Hz, the total discharge amplitude shows a gradual drop. Under 800 Hz and 1 kHz, there is a nonlinear trend, and the minimum total discharge amplitude appears at 10 kPa. The total discharge amplitude per second shows a peak at 30 kPa for different frequencies. Consequently, conducting insulation evaluation under a suitable low pressure (such as 30 kPa) contributes to improve the overall strength of the MEA insulation system.

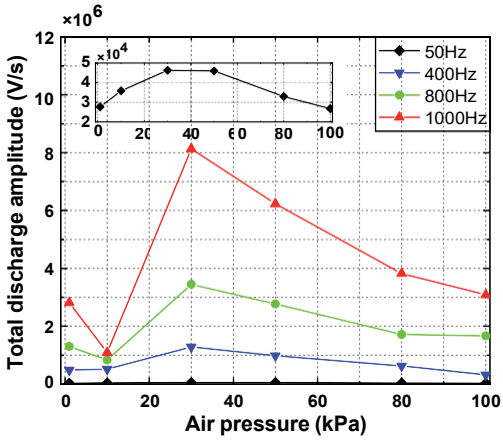

Figure 8. Accumulated discharge amplitude versus air pressure under different frequencies.

Aiming to understand why the damage caused by high frequency varies significantly, further information, in the form of the discharge repetition rate, is given as Figure 9. Variation under different air pressure can also be divided into 30–101 kPa and 1–10 kPa. When air pressure falls in the range of 30–101 kPa, the discharge repetition rate gradually increases with air pressure decreasing, and the highest discharge repetition rate of

PD appears at 30 kPa. The discharge repetition rate shows a "U"-shaped change pattern under 1–10 kPa, with the minimum value at 10 kPa. As the frequency increases, the discharge repetition rate is multiplied, which means that under the same voltage amplitude, high frequency causes more severe insulation damage in MEA.

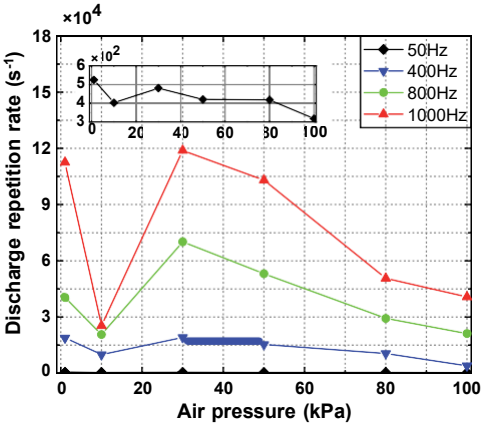

Figure 9. Discharge repetition rate versus air pressure under different frequencies.

3.3 PRPD FEATURE AT DIFFERENT AIR PRESSURE AND FREQUENCIES

To investigate the statistical features and information on phase of partial discharge, the PD data of 200 consecutive cycles was used to plot PRPD spectrum, and the PRPD at various air pressure and frequencies is drawn in Figures 10 and 11. Figure 10 shows the PRPD at different air pressure under 50 Hz. As the air pressure decreases, the PRPD gradually becomes denser, and the spectrum in the positive cycle is basically the same as negative cycles. At 101 kPa and 80 kPa, the shape of PRPD displays an isosceles triangle "▲". As the air pressure drops to 50 kPa, the PRPD begins to be a right triangle "◣". PRPD shape is presented as right triangle "◣" with pressure below 50 kPa. The phase shift is also closely related to the air pressure. The graph shows that there has been a marked shift in PRPD phase. At 30 kPa, the discharge pulse starts to appear at the left of the zero-crossing point, and then the offset gradually increases. In the phase width, there is a slight rise with the decrease of air pressure. The phase width of the positive cycle is 108.99° at atmospheric pressure, and it increases to 114.46° at 1 kPa.

Figure 11 illustrates the PRPD at a frequency of 1 kHz. There are a number of similarities between 50 Hz and 1 kHz, including the shape of the PRPD under the pressure of 101 kPa demonstrates a triangle "▲", gradually turning to right triangle "◣" as the pressure decreases. The number of peaks has been found that it gradually changes from one to two as the air pressure drops. When the pressure is 30 kPa, the PRPD has shown two obvious peaks of equal height. As the pressure drops to 1 kPa, the PRPD again reveals an obvious feature of "single peak." The phase shift and width at 1 kHz are greater than 50 Hz with the same trend. The initial phase of the negative period is 151.42°, and the discharge phase width is 120.14° at 1 kPa.

It can be seen from Figure 10 and Figure 11 that the frequency has a promoting effect on the PRPD. At 50 Hz, the discharge pulses begin to appear at the left of the zero-crossing point under 30 kPa, while at 1 kHz there are many PD pulses at the left of the zero-crossing point under 50 kPa. In addition, the shape at 1 kHz is more abundant than 50 Hz. The testing results indicate the important impact of frequency on PD. Moreover, it makes a possibility to recognize the discharge under different working conditions.

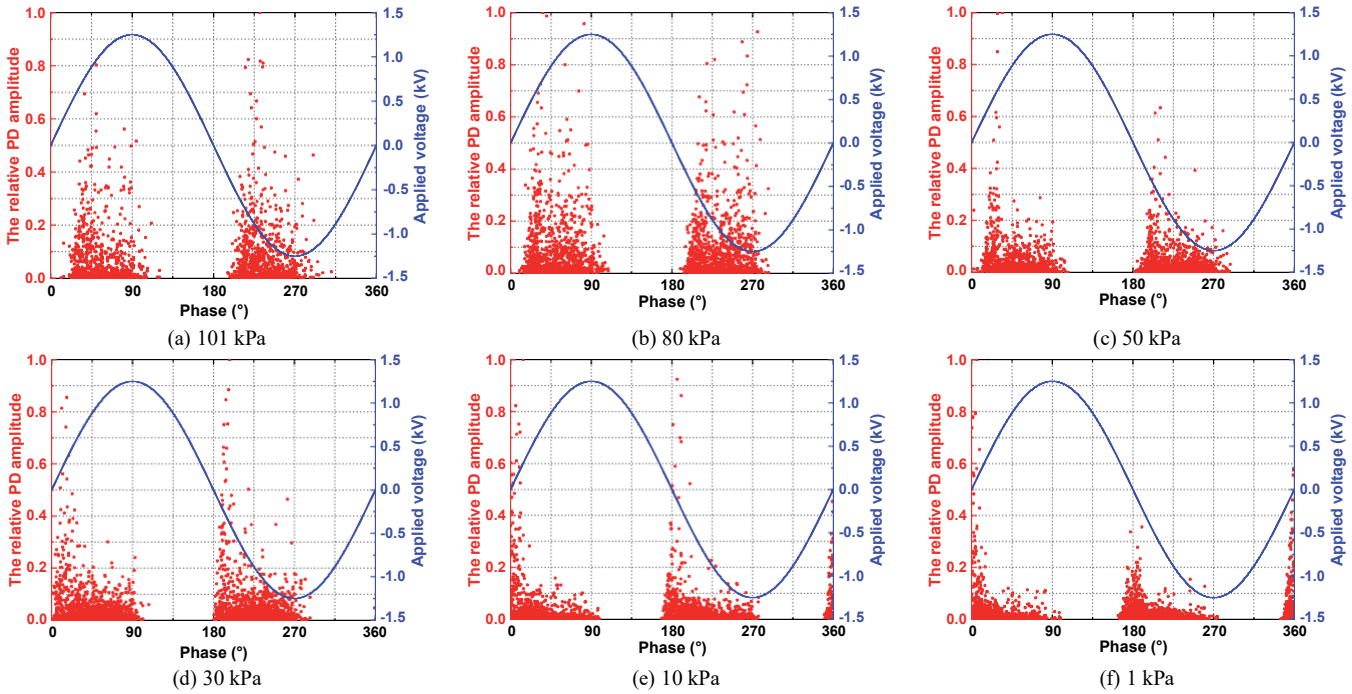

(a) 101 kPa (b) 80 kPa (c) 50 kPa

(d) 30 kPa (e) 10 kPa (f) 1 kPa

Figure 10. The PRPD at different air pressure under 50 Hz.

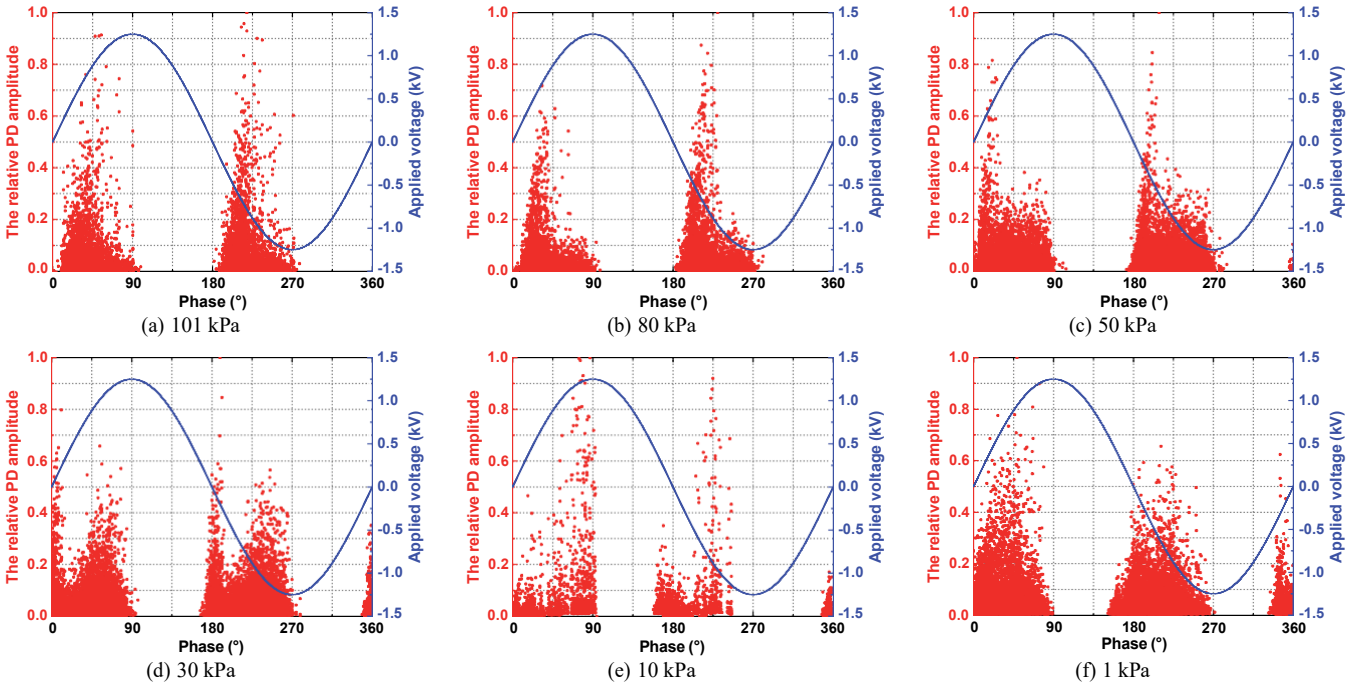

(a) 101 kPa (b) 80 kPa (c) 50 kPa

(d) 30 kPa (e) 10 kPa (f) 1 kPa

Figure 11. The PRPD at different air pressure under 1 kHz.

4 ANALYSIS AND DISCUSSION

4.1 THE LOCATION OF PD

Before exploring the influence mechanism of air pressure on partial discharge, we need to know the location of PD. As we know, the voltage is divided according to its relative dielectric constant. The smaller the relative dielectric constant, the greater the voltage divided. The relative dielectric constant of air is about 1, and the relative dielectric constant of polyimide is about 3.4. Therefore, the intermediate air gap bears a much higher voltage than the insulating layer, and the electric field intensity of the air gap is much larger than that of the insulating layer, so the PD first occurs in the air gap. In addition, the PD not only cause changes in voltage and current waveforms, but also changes in sound, light and heat. The position of the corona can be used to determine the location of PD. A miniature camera installed on the experimental platform is used to take images of the PD under low air pressures in a dark environment, as shown in Figure 12. It clearly shows the occurrence of PD in the fault model.

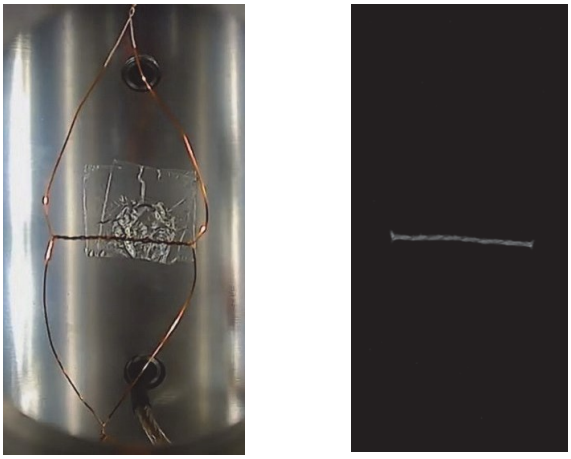

(a) PD model (b) 10 kPa

Figure 12. PD model and the image at 10 kPa.

4.2 THE INFLUENCE OF AIR PRESSURE ON THE AMPLITUDE AND NUMBER OF DISCHARGE

In order to determine the influence of air pressure on amplitude and number of discharges, the charge and electric field models under sinusoidal voltage is established in Figure 13, where E_a is the applied field strength brought by the applied voltage, E_q is the charge electric field intensity caused by the accumulation of charge during discharge, and E_i is the intensity of the superimposed electric field. The two electromagnetic wires are assumed to be A and B. The electrons and ions are produced in the air gap by partial discharge, and the polarity, position, movement speed of the electric charges have a great influence on electric field. When the alternating current (AC) voltage is applied, there is a polarity change in zero-crossing point. Since the electric charges take some time to move, there is some phase that the polarity of electric charges is opposite to applied voltage. After this, the polarity of electric charges changes as moving and neutralizing due to discharge. This process promotes or inhibits the occurrence of PD under different phases. According to the different positions of the sinusoidal voltage, the discharge process in one cycle can be divided into 4 stages.

Stage 1. The first stage locates at the right of zero-crossing point of the positive cycle. The polarity of the applied electric field is turned while the electric charges remain. This results in the superposition of the applied electric field E_a and the charge electric field E_q, i.e., $E_i = E_a + E_q$. E_q strengthens the air gap field strength and promotes the discharge.

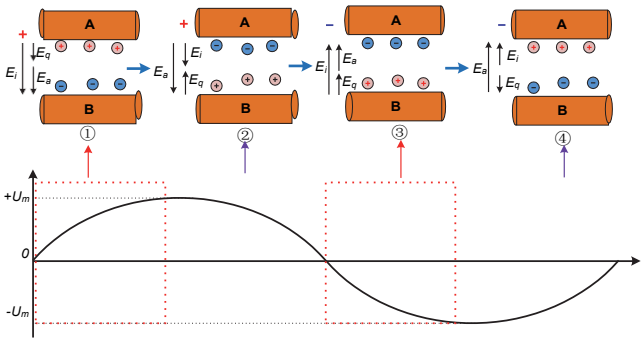

Figure 13. The electric field change process in a sine cycle.

Stage 2. The second stage locates at the second half of the positive cycle. Due to the movement of accumulated charges, a charge electric field E_q is generated in the air gap, and E_q is opposite to the external electric field E_a. At this time, $E_i = E_a - E_q$, E_q weakens the air gap field strength and suppresses the production of PD pulses.

The electric field changes of **Stage 3** and **Stage 4** are the same as **Stage 1** and **Stage 2,** respectively, but in opposite directions. Therefore, repeated analysis is not necessary.

In order to combine electric field and discharge pulses, the electric field and pulses model in the air gap are shown in Figure 14, where E_{min} is the minimum discharge field strength of the air gap, E_{res} is the residual air gap field strength after discharge, $\triangle E$ is the difference between the air gap electric field intensity and the minimum discharge electric field intensity, t_e is the effective discharge time on the condition that the applied field is stronger than the minimum electric field leading to discharge of the air gap, t_{de} is the discharge delay time, and t_r is the air gap recovery time. The discharge amplitude is closely related to E_{min}, ΔE and t_{de}, and the number of discharges is closely related to t_e and t_r.

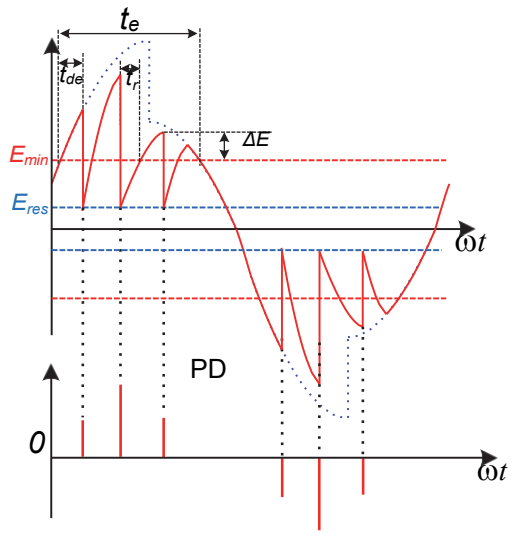

Figure 14. The model of air gap electric field intensity variation and discharge pulse.

As the air pressure decreases, the PDIV changes in direct proportion to the air pressure. It is easy to know that Emin and Eres have the same trend with PDIV. Therefore, as the air pressure decreases, E_{min} and E_{res} also decrease. The smaller E_{res} and greater ΔE caused by low air pressure result in a higher discharge amplitude. On the other hand, the decrease of E_{min} makes the initial electrons more easily excited, reducing t_{de} and the PD amplitude. The combined effect of the two aspects constitutes the influence mechanism of air pressure on the PD amplitude. When the air pressure is 30–101 kPa, the influence of E_{res} is slightly greater, causing a certain fluctuation or even a slight increase in the discharge amplitude. When the air pressure is below 30 kPa, the initial electrons are easily excited, and the discharge amplitude is significantly reduced.

The number of discharges is determined by t_e and t_r. On the one hand, the reduction of E_{min} elongates the effective discharge time t_e, which could increase the number of discharges. On the other hand, the reduction of E_{min} reduces t_r, which shortens the discharge time of a single pulse. The extension of the effective discharge time and the shortening of the single discharge time under low air pressure together led to an increase in the number of PD.

4.3 THE INFLUENCE OF AIR PRESSURE ON THE CHARACTERISTICS OF PRPD

PRPD cannot only display information, such as the phase and statistical shape of the discharge, but also can be used as a feature for pattern recognition of discharge and fault diagnosis. Based on the analysis of Section 3, the characteristics of the PRPD affected by air pressure are mainly as follows:

- Phase shift: As the air pressure decreases, the PRPD shifts to the left. The lower the air pressure, the greater the offset;
- Phase width: As the air pressure decreases, the discharge phase width gradually increases;
- Shape characteristics: With the decrease of air pressure, the number of PRPD peaks changes from one to two, and a "rabbit ear" shape appears. As the air pressure continues to drop, the number of peaks gradually changes from two to one again.

The PDIV and the reversal time of the accumulated charges under different air pressure have a great influence on the discharge spectrum. The reduction of PDIV at low pressure decreases the E_{min}. According to Figure 14, the t_e increases with reduction of the E_{min}, which would advance the generation phase of the PD pulses and increase the phase width. Therefore, the PRPD shows a trend of shifting to left and phase width increase with the decrease of air pressure.

In order to explain the PRPD shape at different pressures, the discharge areas at different phases are established. Figure 15 shows the variation model of the applied field strength and the air gap field strength under different pressures, where $p_{(a)} > p_{(b)} > p_{(c)}$, area I is the discharge area formed by the E_q and the E_a in the same direction, area II is the discharge area formed by the reverse addition of the E_q and the E_a. When the direction of the E_q is the same as the E_a, the charges generated by the discharge neutralize the accumulated charge and promote the polarity reversal of E_q. Therefore, the discharge pulses accelerate the polarity reversal of E_q, and the earlier the discharge occurs, the sooner the reversal of E_q is completed. As the discharge pulses

shifts to the left, the reversal of E_q is completed earlier at low air pressure that affects the distribution of the discharge areas. In atmospheric pressure, the discharge mainly occurs in the area I because of the high level of E_{min}, shown in Figure 15a. The air gap electric field has only one peak, so the characteristic of a single peak is presented in PRPD. As the air pressure gradually decreases, the electric field is as shown in Figure 15b. E_{min} decreases and the polarity reversal of E_q is completed earlier. The air gap field rises to a high point in area I and area II, respectively, which both are above E_{min}. So, the shape characteristic of "double peak" is shown in PRPD. In addition, there is some phase area that E_i is greater than E_{min} in the left of zero-crossing point, which makes the discharge phase shift beyond the voltage zero-crossing point. The electric field under a lower air pressure is shown in Figure 15c. The discharge area can be clearly separated into two parts. Area I gradually shrinks or even disappears, area II gradually expands. Therefore, the characteristic of "single peak" is obvious in PRPD again.

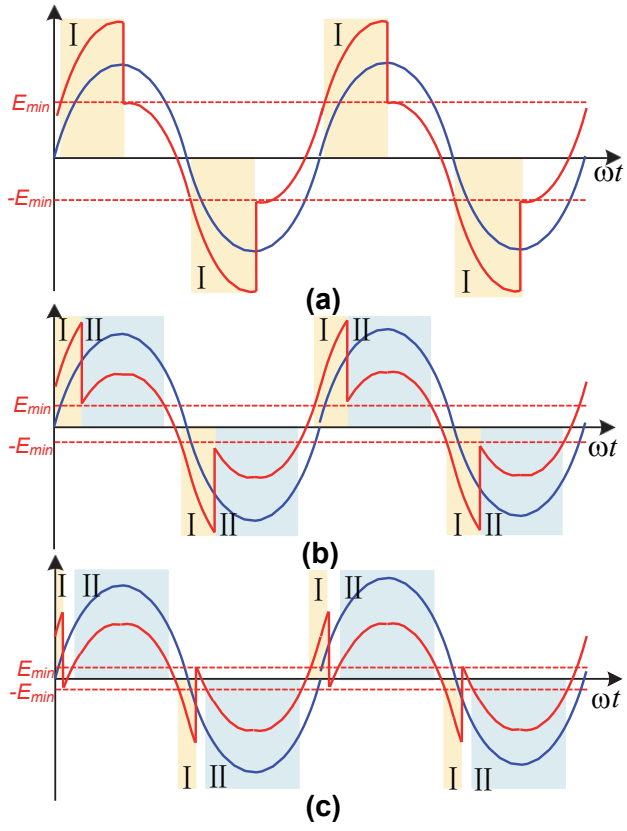

Figure 15. Variation model of applied field strength and air gap field strength under different pressures, $p_{(a)} > p_{(b)} > p_{(c)}$.

5 CONCLUSIONS

As future MEAs are heading towards higher AC power generation and more optimum architectures, it is extremely important to understand the partial discharge behavior under more challenging operating systems. This paper investigates the behavior of PD in atmospheric air as a function of frequencies up to 1 kHz. The main conclusions obtained are as follows:

1) Low air pressure has a reduction effect on PDIV. The PDIV decreases linearly as the air pressure decreases, and the PDIV at 1 kPa is less than 50% of its level at atmospheric pressure; the frequency has no significant effect on PDIV in the range of 50–1000 Hz. Therefore, the insulation of MEA under low air pressure should be paid more attention during the design and operation.

2) Air pressure and frequency have a great influence on the amplitude and number of discharges. As the pressure decreases, the discharge amplitude fluctuates and the number of discharges gradually increases in the air pressure range of 30–101 kPa, while the discharge amplitude and number tend to decrease during 1–30 kPa. As the frequency increases, the number of discharges gradually increases. The highest total discharge amplitude appears under the combination of 30 kPa and 1 kHz, indicating that low air pressure and high frequency bring more severe damages to insulation of MEA.

3) Air pressure and frequency affect the shape, number of peaks and phase distribution of the PRPD. As the air pressure decreases, the shape of the PRPD undergoes four changes of "▲" → "◣" → "▲▲" → "▲", and the number of peaks experiences a change of "single peak" → "double peak" → "single peak". The lower the pressure, the greater the PRPD phase width and phase shift. High frequency promotes the characteristic change of the PRPD. The shape of the PRPD at 50 Hz is only "▲" → "◣", while it shows four shapes at 1 kHz. This makes a possibility to diagnose the discharge under different air pressure and frequencies.

ACKNOWLEDGMENT

This work is supported by the Natural Science Foundation of Jiangsu Province (SBK2021020744) and the Fundamental Research Funds for the Central Universities (NT2021012). The authors also gratefully acknowledge financial support from NUAA International Cooperation Seed Fund.

REFERENCES

[1] J. Chen, C. Wang and J. Chen, "Investigation on the Selection of Electric Power System Architecture for Future More Electric Aircraft," IEEE Trans. Dielectr. Electr. Insul., vol. 4, no. 2, pp. 563–576, Jan. 2018.

[2] B. Sarlioglu and C. T. Morris, "More Electric Aircraft: Review, Challenges, and Opportunities for Commercial Transport Aircraft," IEEE Trans. Transp. Electrif., vol. 1, no. 1, pp. 54–64, May. 2015.

[3] Z. Zhang *et al*, "Overview and development of variable frequency AC generators for more electric aircraft generation system," Chin. J. Electr. Eng., vol. 3, no. 2, pp. 32–40, Sep. 2017.

[4] V. Madonna, P. Giangrande and M. Galea, "Electrical Power Generation in Aircraft: Review, Challenges, and Opportunities," IEEE Trans. Transp. Electrif., vol. 4, no. 3, pp. 646–659, May. 2018.

[5] A. Barzkar and M. Ghassemi, "Electric Power Systems in More and All Electric Aircraft: A Review," IEEE Access, vol. 8, pp. 169314–169332, Sep. 2020.

[6] J. K. Nøland *et al*, "High-Power Machines and Starter-Generator Topologies for More Electric Aircraft: A Technology Outlook," IEEE Access, vol. 8, pp. 130104–130123, Jul. 2020.

[7] E. H. N. Diaw *et al*, "Current Measurements in High Performance Polymers Used in Aeronautic Cables," IEEE Trans. Dielectr. Electr. Insul., vol. 27, no. 6, pp. 2195–2202, Dec. 2020.

[8] W. Li, I. Cotton and R. Lowndes, "Development of a Test Method for Validation of Creepage Distances in High Voltage Aerospace Power Systems," *2020 IEEE Electrical Insulation Conference (EIC)*, 2020, pp. 517–520.

[9] B. H. Nya, J. Brombach and D. Schulz, "Benefits of higher voltage levels in aircraft electrical power systems," *2012 Electrical Systems for Aircraft, Railway and Ship Propulsion (ESARS)*, 2012, pp. 1–5.

[10] E. Sili *et al*, "Polyimide lifetime under partial discharge aging: effects of temperature, pressure and humidity," IEEE Trans. Dielectr. Electr. Insul., vol. 20, no. 2, pp. 435–442, May 2013.

[11] E. Sili and J. P. Cambronne, "About the validity of lifetime models of polymers under electrical discharge in aeronautical environment," *2013 Annu. Rep. Conf. Electr. Insul. Dielect. Phenom. (CEIDP)*, 2013, pp. 1306–1309.

[12] A. Driessen, J. Van Duivenbode and P. Wouters, "Partial discharge detection for characterizing cable insulation under low and medium vacuum conditions," IEEE Trans. Dielectr. Electr. Insul., vol. 25, no. 1, pp. 306–315, Mar. 2018.

[13] M. G. D. L. Calle *et al*, "Uncertainty Sources in the Estimation of the Partial Discharge Inception Voltage in Turn-to-Turn Insulation Systems," IEEE Access, vol. 8, pp. 157510–157519, Aug. 2020.

[14] L. Lusuardi *et al*, "Insulation design of low voltage electrical motors fed by PWM inverters," IEEE Electr. Insul. Mag., vol. 35, no. 3, pp. 7–15, May 2019.

[15] C. V. D. Steen, C. Abadie and G. Belijar. "Partial discharge detection, Experimental-Simulation Comparison and actual limits," *2020 IEEE Electrical Insulation Conference (EIC)*, 2020, pp. 537–541.

[16] R. Rui and I. Cotton, "Impact of low pressure aerospace environment on machine winding insulation," *2010 IEEE International Symposium on Electrical Insulation*, 2010, pp. 1–5.

[17] Z. Shi *et al*, "The 3D φ-n-q Analysis of Partial Discharge Detection in Low Pressure Conditions," *2019 29th Australasian Universities Power Engineering Conference (AUPEC)*, 2019, pp. 1–5.

[18] Y. Wang *et al*, "Partial Discharge Investigation of Form-Wound Electric Machine Winding for Electric Aircraft Propulsion," IEEE Trans. Transp. Electrif., vol. 6, no. 4, pp. 1638–1647, Mar. 2020.

[19] F. Alrumayan, I. Cotton and A. Nelms, "Partial Discharge Testing of Aerospace Electrical Systems," IEEE Trans. Aerosp. Electron. Syst., vol. 46, no. 2, pp. 848–863, May 2010.

[20] J. Jiang *et al*, "Optical Sensing of Partial Discharge in More Electric Aircraft," IEEE Sens. J., vol. 20, no. 21, pp. 12723–12731, Jun. 2020.

[21] J. Auersvald and K. Draxler, "Aerometric system for general aviation," *International Conference on Military Technologies (ICMT)*, 2015, pp. 1–6.

[22] M. Florkowski, B. Florkowska and P. Zydron, "Partial discharge forms for DC insulating systems at higher air pressure," IET Sci. Meas. Technol., vol. 10, no. 2, pp. 150–157, Mar. 2016.